Journal of Robotics and Control (JRC)
Volume 6, Issue 3, 2025
ISSN: 2715-5072, DOI: 10.18196/jrc.v6i3.26868

Passivity-Preserving Reduction of High-Order Electro-Mechanical Robot Systems

Manh-Quan Nguyen [1], Anh-Tuan Vu [2], Trung-Kien Ha [3], Hong-Quang Nguyen [4*]
[1, 2, 3] Hanoi University of Industry, Hanoi, Vietnam
[4] Thai Nguyen University of Technology, Thai Nguyen, Vietnam
Email: [1] quannm@haui.edu.vn, [2] tuanva@haui.edu.vn, [3] hatrungkien@haui.edu.vn, [4] quang.nguyenhong@tnut.edu.vn
*Corresponding Author

Abstract*—High-order electro-mechanical robot systems (EMRS) present formidable challenges in real-time simulation and embedded control due to their substantial state-space dimensionality and tightly coupled multi-domain dynamics. Excessive model complexity impedes rapid simulation and controller synthesis exacerbates computational demands in resource-constrained environments. This study systematically investigates passivity-preserving model order reduction (PP-MOR) for electro-mechanical robot systems, prioritizing the retention of essential dynamic fidelity and energy dissipation. In contrast to standard balanced truncation or Krylov subspace approaches, the PP-MOR algorithm maintains physical consistency and achieves an optimal balance between model simplicity and dynamic accuracy. This method that employs positive-real algebraic Riccati equations to compute system Gramians, utilizes congruence transformations for system balancing, and imposes constraints to ensure both stability and strict passivity in the reduced-order models. Reduction experiments on the eight-state EMRS benchmark produced models of orders one, two, and four. The fourth-order model achieved H_2 and H_∞ errors of 7.2×10^{-4} and 8.5×10^{-4}, respectively, with time-domain metrics, ISE, IAE, ITAE, and RISE, remaining below 1.1×10^{-4}. Both second-order and third-order reductions yielded errors under 10^{-1} across all criteria, while first-order truncation resulted in a tenfold increase in worst-case gain mismatch (0.82 vs. 0.07 for fourth order) and significant transient deviations. The fourth-order model also preserved key dynamic features, including resonance peak, bandwidth, phase margin, and step response overshoot, with less than 0.5% deviation from the original system. By enabling simulation and embedded implementation of EMRS models, this approach paves the way for advanced robotic applications in manufacturing and autonomous systems, where computational efficiency and robust performance are paramount.

Keywords—Balanced Truncation; Electro-Mechanical Robotics; Error Norms; Model Order Reduction; Riccati Equations.

I. INTRODUCTION

Electro-mechanical robot systems (EMRS) represent a sophisticated integration of electrical power converters, advanced control electronics, and diverse actuators, including servo motors, ball-screw drives, and electromagnetic elements, within mechanical structures to achieve programmable, high-precision, and repeatable motion [1], [2]. Foundational dynamic models, often formulated through coupled differential equations and implemented in MATLAB toolboxes, enable accurate simulation and validation of motion control strategies [3]–[5]. The Lagrange–Maxwell formalism and related approaches have been widely adopted to capture global electromechanical coupling, facilitating prediction of dynamic responses and vibration characteristics in both rigid and flexible manipulators [6]–[9].

The versatility of EMRS is evident in the breadth of actuation schemes, from magnetic dampers for vibration control to high-articulation wrist assemblies for surgical robotics, and continuum robots employing electromagnets and springs for multi-degree-of-freedom bending [10]–[14]. Research on energy-efficient operation has emphasized the importance of electromechanical identification and dynamic optimization to reduce overshoot, settling time, and power consumption during trajectory execution [15]–[18]. The introduction of electromechanical brakes, clutches, and novel actuation mechanisms such as electrostatic bellows and capstan clutch multiplexers has enabled lightweight, dexterous, and scalable robotic platforms [19]–[23]. At smaller scales, electromagnetic microrobotic systems leverage wireless actuation for targeted interventions, notably in cardiovascular procedures, where operator safety is paramount [24]–[26]. The potential applications of EMRS span a wide technological spectrum. Hybrid electromagnetic and triboelectric sensors support self-powered balancing platforms, while integrated electromechanical servo systems optimize mass and volume for aerospace and mobile robotics [27]–[31]. Electro-hydraulic actuators, brake-by-wire systems, and FPGA-based electric arms with embedded image processing have advanced both industrial automation and heavy-duty collaborative robotics [32]–[36]. Innovations in soft robotics, such as stretchable electret films for simultaneous sensing, actuation, and energy harvesting, have paved the way for multifunctional manipulators and wearable devices [37]–[40]. Electromagnetic wheel robots and miniaturized floating robots further extend EMRS capabilities to inspection, maintenance, and micro-scale assembly in challenging environments [41]–[45]. In rehabilitation and assistive domains, smart wheelchair robots equipped with voice, gesture, and GPS integration restore mobility and independence, while wheelchair-mounted robotic arms facilitate daily tasks with seamless positioning [46]–[50]. Redundant manipulators with high degrees of freedom have proven essential for disaster relief and search-and-rescue operations in unstructured settings [51]–[54]. Advanced control schemes, including adaptive parallel iterative learning, reinforcement learning–based Stewart platform controllers, and vision-based visual servoing using YOLOv5, have significantly improved precision and

adaptability in repetitive and complex tasks [55]–[59]. Fuzzy logic, nonlinear model predictive control, and swarm-based multi-agent coordination have enhanced obstacle avoidance, navigation, and mission execution in hazardous environments [60]–[64]. The integration of IoT platforms, hybrid LQR-fuzzy-PID schemes, and variable-stiffness actuators continues to accelerate the deployment of EMRS in agriculture, logistics, and medical rehabilitation [65]–[69].

With the increasing complexity and functionality of EMRS, high-order state-space models, often comprising hundreds of coupled variables, have become essential for capturing intricate system behaviors [70]–[74]. However, such models impose substantial computational burdens on simulation, parameter identification, and real-time control [75]–[78]. The challenge of balancing model fidelity with computational tractability is particularly acute in embedded and resource-constrained environments, where excessive model order can render advanced control strategies impractical [79]–[82]. Moreover, simplification via dimension reduction or partial linearization, while alleviating computational load, may exacerbate sensitivity to parameter uncertainties and compromise key properties such as stability and passivity [83]–[87].

Traditional model order reduction (MOR) techniques, including balanced truncation and Krylov subspace methods, provide partial solutions by reducing system dimensionality [88]–[92]. Yet, these approaches often fail to preserve passivity, a critical property for ensuring energy dissipation and closed-loop stability, thereby limiting their effectiveness in safety-critical and energy-aware EMRS applications [13], [34], [55], [76], [89]. Recent research efforts have introduced advanced abstraction methods, neural ODE frameworks, and mathematical tools such as Lie-group kinematics and Möbius-inversion-based formulations to enhance modeling efficiency and expressivity [63], [66], [73], [75], [77]. However, these innovations frequently entail significant analytical or computational overhead and may not guarantee the retention of essential physical properties as system order increases [67], [68], [71], [74], [77].

To address these limitations, passivity-preserving model order reduction (PP-MOR) algorithms have emerged as a robust solution for reducing the dimensionality of high-order EMRS while strictly maintaining stability and passivity [78]–[81]. Conic positive-real balanced truncation extends standard approaches by introducing phase-angle constraints, thereby enhancing reduction accuracy for linear time-invariant passive subsystems [78], [79], [84], [85], [90]. High-performance implementations employ quadratic alternating-direction implicit iteration to efficiently solve algebraic Riccati equations, reducing memory requirements and enabling large-scale order reduction [80], [81], [88], [89]. Mixed balanced truncation techniques unify Gramian-based and Riccati-based methods to achieve concurrent passivity and numerical robustness with lower computational cost [82], [83], [86], [87], [91]. Extensions such as phase-preserving, frequency-weighted, and reciprocal positive-real balanced truncation further tailor reduced models to stringent transient, bandwidth, and descriptor-form requirements typical of EMRS applications [84]–[90].

Despite these methodological advances, a critical need remains for systematic evaluation of PP-MOR algorithms on realistic, high-order EMRS platforms, with a focus on quantifying the trade-offs between model simplicity, dynamic fidelity, and physical consistency [1], [12], [39], [56], [91]. In this context, the present study investigates the application of a passivity-preserving balanced truncation algorithm to a benchmark high-order EMRS model [91], [92]. By leveraging positive-real algebraic Riccati equations, congruence transformations, and explicit phase-angle constraints, the proposed method produces reduced-order models that retain the original system's frequency- and time-domain characteristics under bounded inputs, while strictly guaranteeing both stability and passivity [78], [79], [80], [81], [91]. This approach not only simplifies controller synthesis and embedded implementation but also enhances reliability and robustness in resource-limited EMRS deployments [65], [70], [88], [90], [92].

The research contribution of this work is the development and rigorous evaluation of a MATLAB based passivity preserving balanced truncation algorithm for high-order EMRS. The proposed method systematically preserves both stability and passivity by leveraging positive-real algebraic Riccati equations, congruence-based balancing, and phase-angle enforcement, thereby advancing the state of the art in model order reduction for safety- and stability-critical robotic applications [78], [80], [83], [86], [91].

II. RESEARCH METHODS

A. *Passivity-Preserving Model Order Reduction (PP-MOR) Algorithm*

The passivity-preserving model order reduction (PP-MOR) algorithm provides a systematic framework for deriving low-order approximations of high-dimensional linear time-invariant (LTI) systems while rigorously maintaining both stability and passivity, two critical properties for robust control and safe physical interaction in electro-mechanical robot systems. The method leverages the solution of two coupled positive-real algebraic Riccati equations to construct generalized Gramians, which encode the system's energy storage and dissipation characteristics. This section offers a concise yet comprehensive breakdown of the algorithm, clarifies its practical implications, and addresses key methodological concerns to support reproducibility and reliability [81].

The PP-MOR algorithm is described as in Fig. 1, specifically:

Inputs:

– State matrices (A, B, C, D)describing in (1)

$$\dot{x} = Ax + Bu; y = Cx + Du \quad (1)$$

– Desired reduced order r < n.

Outputs: Reduced matrices (A_r, B_r, C_r, D_r) that preserve stability and passivity.

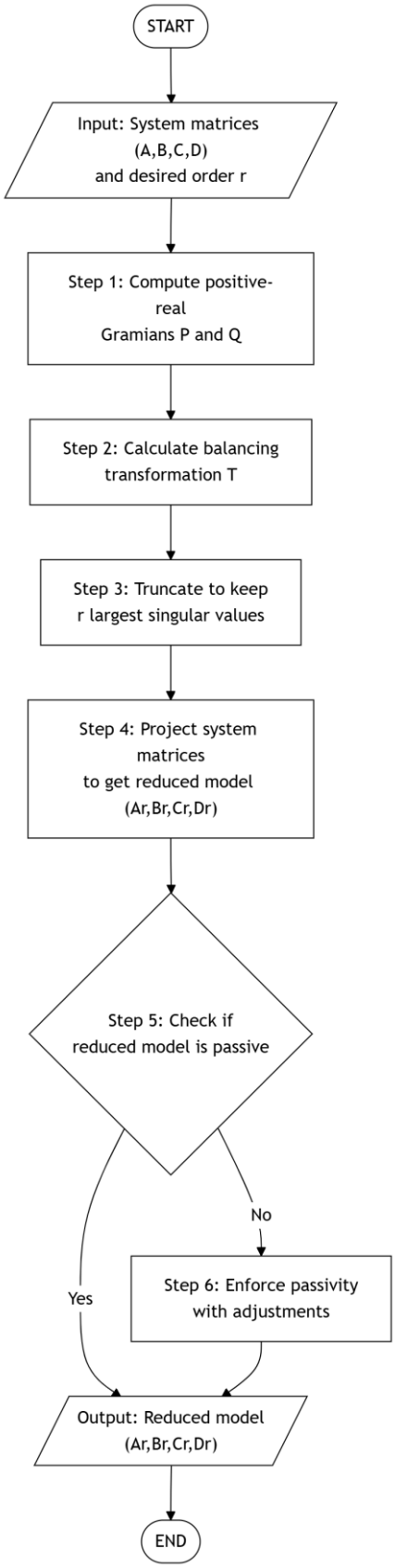

Fig. 1. PP-MOR Algorithm flow chart

Step-by-Step description:

1. Compute Positive-Real Gramians: Solve (2) and (3) to obtain P and Q, when $U = (D + D^T)^{-1}$.

$$AP + PA^T + (PC^T - B)U^{-1}(PC^T - B)^T = 0 \quad (2)$$

$$A^TQ + QA + (B^TQ - C)^TU^{-1}(B^TQ - C) = 0 \quad (3)$$

The existence and uniqueness of solutions depend on the system's minimality and positive-realness. Numerical solvers should employ robust algorithms (e.g., Schur or Newton-Kleinman methods) with appropriate stopping criteria (typically relative residuals below 10^{-8}) to guarantee convergence. Regularization or preconditioning is necessary for ill-conditioned or nearly singular systems.

2. Compute a congruence transformation T that simultaneously diagonalizes P and Q: $T^TPT = T^{-1}Q(T^{-1})^T = \Sigma$, where Σ is a diagonal matrix of positive singular values. This transformation aligns the energy metrics of controllability and observability, facilitating a balanced representation of the system's dynamic modes. Ill-conditioning may arise if the original system exhibits widely disparate time constants or poorly separated modes. In such cases, singular value decomposition (SVD) or regularized balancing transformations can improve numerical stability.

3. Truncate low-energy modes: Partition $\Sigma = \text{diag}(\Sigma_r, \Sigma_{n-r})$ and retain the first *r* largest singular values. This step reduces the model order while preserving the dominant energy pathways. Truncating low-energy modes accelerates simulation and controller synthesis but may attenuate high-frequency or weakly observable dynamics. Careful selection of r based on Hankel singular value decay and application-specific performance criteria is essential to balance accuracy and efficiency.

4. The original state-space matrices $(A, B, C, D)$are projected onto the reduced subspace using the leading columns of *T*, yielding the reduced-order matrices (A_r, B_r, C_r, D_r). To maintain physical interpretability, one should verify that the reduced matrices preserve essential structural properties, such as symmetry or sparsity, if present in the full-order model.

5. Adjust and if necessary, apply a constraint so that (A_r, B_r, C_r, D_r) remains positive-real.

This procedure yields a reduced EMRS model that accelerates simulation, simplifies controller design, and guarantees the original system's passive stability. Truncation directly impacts the fidelity of transient and steady-state responses; retaining too few modes can degrade disturbance rejection or control precision. Careful parameter selection, sensitivity analysis, and validation against experimental or high-fidelity simulation data are crucial to confirm that the reduced-order model meets application-specific requirements.

B. Electro-Mechanical Robot System Modeling

The electro-mechanical robot system (EMRS) considered in this study integrates mechanical, electrical, and control subsystems within a unified state-space framework. The modeling approach seeks to capture the essential dynamics of each physical domain and their interactions, enabling accurate simulation and informed controller design. However, it is important to critically assess the modeling

assumptions, state selection, and potential limitations to ensure that the resulting model is both representative and suitable for subsequent model reduction. The EMRS under consideration is depicted in Fig. 2, which integrates electrical and mechanical components to realize motion control in a robot. The system comprises the following functional blocks [92]:

(B1) Pressure Sensor: The pressure sensor is modeled as a second-order mass-spring-damper mechanical system that converts force into deformation, and subsequently into a voltage signal via piezoresistive transduction.

(B2) Inverting Operational Amplifier: amplifies the transduced voltage.

(B3) Controller: processes the amplified signal to generate a control voltage.

(B4) Servo Motor: converts electrical energy into rotational mechanical motion.

(B5) Robot Body: transforms motor shaft rotation into linear motion of the robot's center of mass (COM).

The system exhibits a multi-domain coupling, requiring dynamic models for both electrical and mechanical domains and their interconversion.

The state vectors

where: $\boldsymbol{x}^T = [z_s \quad \dot{z}_s \quad x_c \quad x_i \quad I_m \quad \omega_m \quad \theta_m \quad e]$

z_s (m) and $\dot{z}_s$ (m/s) are the displacement and velocity of the pressure sensor's proof mass;

x_c (V) is the internal voltage state of the inverting amplifier (first order);

x_i (V·s) is the integrator state in the PI controller;

$I_m(A), \omega_m(rad/s), \theta_m(rad)$ are the motor current, angular velocity, and shaft angle;

$e = V_{\text{ref}} - V_s e = Vref$ is the control error.

The input is the reference voltage $Vref$ and the measured output is the motor torque proportional signal: $y = K_t I_m$ (K_t: Torque constant).

The eight selected state variables represent essential physical quantities governing the system's energy and signal pathways, ensuring accurate capture of inter-domain dynamics and effective passivity preservation during reduction. Alternative representations, such as modal or aggregated forms, were evaluated but found less suitable for maintaining passivity and physical interpretability.

The model assumes ideal transduction and omits parasitic effects (e.g., friction, hysteresis, sensor noise, actuator saturation) for analytical clarity. While these simplifications facilitate tractability, they may affect predictive accuracy in practical scenarios. The strong coupling between electrical and mechanical domains can introduce numerical stiffness, which requires careful scaling or, if necessary, time-scale separation. For higher-fidelity applications, incorporating unmodeled dynamics and validating against experimental data are recommended to ensure robustness.

The chosen state-space formulation and modeling assumptions critically determine the efficacy of PP-MOR. A physically grounded, comprehensive model enables the reduced-order system to retain key properties such as stability and passivity. Conversely, oversimplification or omission of relevant states risks loss of essential dynamics, compromising both theoretical soundness and practical utility.

III. Application of the PP-MOR Algorithm for Order Reduction of the Electro-Mechanical Robot System

We implemented the Passivity-Preserving Model Order Reduction (PP-MOR) algorithm in MATLAB and applied it to the Electro-Mechanical Robot System (EMRS). Reducing the original 8th-order model to order 1 yielded the error metrics and H∞ and H_2 norm plots shown in Table I and Fig. 3, as well as the ISE, IAE, ITAE, and RISE values and corresponding plots in Table II, Fig. 4 and Fig. 5.

The H_2 norm of the error system $\Delta(s) = G(s) - \hat{G}(s)$ measures the energy of the impulse response of $\Delta(s)$. Numerically, $\|\Delta\|_2 = (\frac{1}{2\pi}\int_{-\infty}^{\infty} \text{Tr}(\Delta^*(j\omega)\Delta(j\omega))d\omega)^{1/2}$. It quantifies the average-energy discrepancy across all frequencies. A small H_2 error indicates that the reduced model closely matches the full system's dynamic energy distribution. It is especially relevant when stochastic or broadband excitations are considered.

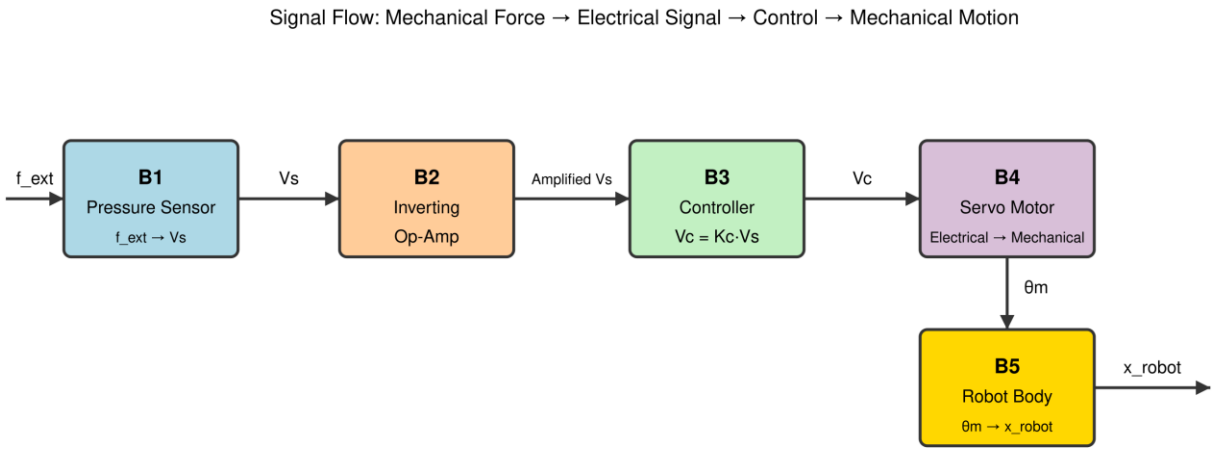

Fig. 2. Electro-mechanical robot system

The H_∞ norm of the error, $\|\Delta\|_\infty = \sup_\omega \sigma_{max}$ represents the worst-case (maximum) gain mismatch across frequencies. Ensuring a low H∞ error guarantees that the reduced model never deviates beyond a specified bound at any frequency. This is critical for robust control design, where worst-case amplification must be limited.

The data in Table I show a clear trend: as the reduced order r increases toward the original order (8), both the H_2 and H_∞ errors decrease monotonically. For high orders (7 and 6), the H_2 error drops below 10^{-3} and H∞ below 5×10^{-4}, indicating excellent fidelity in both energy-norm and worst-case gain metrics. However, orders 1 to 3 exhibit orders of magnitude larger errors, revealing that extremely low-order models cannot capture the full dynamics. Order 5 or above has H_∞ errors below 0.003, which is often acceptable in control design for lightly damped resonant systems.

TABLE I. H_2 AND H_∞ NORM ERRORS VS. REDUCED ORDER

Reduced Order r	H_2 Norm Error	H_∞ Norm Error
7	8.9762×10^{-5}	1.8426×10^{-4}
6	2.5913×10^{-4}	4.6164×10^{-4}
5	1.2967×10^{-3}	2.8741×10^{-3}
4	3.9354×10^{-3}	7.2260×10^{-3}
3	5.2866×10^{-2}	9.4487×10^{-2}
2	5.3309×10^{-2}	9.5143×10^{-2}
1	3.9995×10^{-1}	5.1092×10^{-1}

This plot in Fig. 3 displays the H_2 (blue circles) and H_∞ (red squares) norm errors of the reduced-order models as functions of model order r on a logarithmic scale. Both error metrics decrease monotonically as r approaches the original order (8), with negligible discrepancies ($<10^{-4}$) at r = 7 and r = 6. Notably, orders 1 to 3 exhibit steep error growth, indicating that extremely low-order truncations fail to capture essential dynamics.

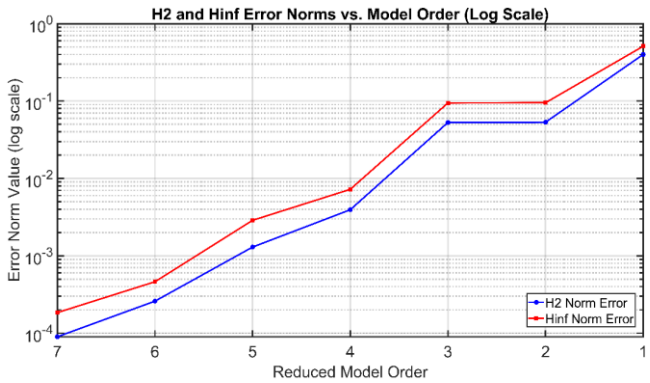

Fig. 3. H_2 and H_∞ error norms vs. model order

Integral of Squared Error $ISE = \int_0^T e^2(t)dt$ where $e(t) = y_{orig}(t) - y_{red}(t)$, it measures total absolute deviation, weighting all errors equally. Low ISE confirms that, in time-domain transient response, the reduced model follows the original trajectory closely, especially during large errors.

Integral of Absolute Error $IAE = \int_0^T |e(t)|dt$ measures total absolute deviation, weighting all errors equally. IAE indicates overall tracking fidelity without over-penalizing spikes; valuable when occasional outliers are less critical.

Integral of Time-Weighted Absolute Error $ITAE = \int_0^T t\,|e(t)|dt$. By weighting errors later in time more heavily, ITAE emphasizes settling performance and steady-state accuracy. Low ITAE shows that the reduced model not only tracks initial transients but also settles to the correct value promptly and remains accurate.

Relative Integral of Squared Error $RISE = \frac{\int_0^T e^2(t)dt}{\int_0^T y_{orig}^2(t)dt}$ normalizes the ISE by the original system's energy, yielding a dimensionless relative error. RISE allows comparing error levels across different operating conditions or plant models by providing a scale-free metric.

TABLE II. TIME-DOMAIN ERROR METRICS VS. REDUCED ORDER

Reduced Order r	ISE	IAE	ITAE	RISE
7	1.67×10^{-8}	4.30×10^{-4}	6.01×10^{-3}	6.02×10^{-8}
6	6.56×10^{-8}	9.22×10^{-4}	1.04×10^{-2}	2.36×10^{-7}
5	3.83×10^{-6}	6.61×10^{-3}	7.50×10^{-2}	1.37×10^{-5}
4	1.55×10^{-5}	1.26×10^{-2}	1.03×10^{-1}	5.55×10^{-5}
3	3.25×10^{-3}	1.76×10^{-1}	1.04	1.17×10^{-2}
2	2.84×10^{-3}	1.46×10^{-1}	6.84×10^{-1}	1.02×10^{-2}
1	4.33	8.89	9.97×10^{1}	1.56×10^{1}

Time-domain metrics in Table II underscore that errors remain negligible for orders ≥ 6 (ISE on the order of $10^{-8} \div 10^{-7}$). Order 5 introduces slight deviation (ISE ≈10^{-6}), still marginal for many applications. Below order 4, all metrics escalate sharply, with RISE indicating significant relative energy discrepancy. The ITAE for order 3 (≈1.04) versus order 4 (≈0.10) highlights that low-order reductions suffer both in early and late transient accuracy.

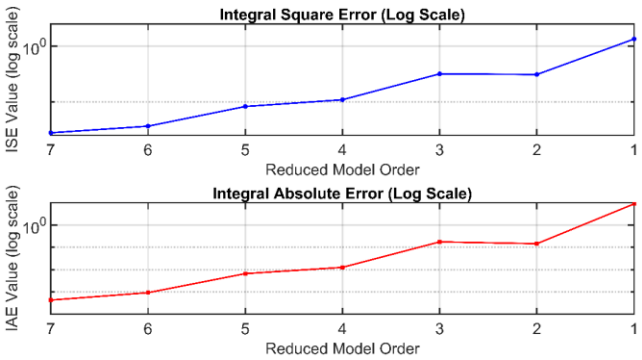

Fig. 4. ISE and IAE vs. model order

The plot in Fig. 4 shows step responses of reduced models. For orders r ≥ 5, ISE remains below 10^{-5} and IAE below 10^{-2}, demonstrating high time domain fidelity. Conversely, orders 1 to 3 produce large errors, confirming insufficient transient tracking at very low.

The Fig. 5 presents the ITAE and the RISE, both on log scales. ITAE remains under 10^{-1} for r ≥ 4, reflecting accurate settling behavior, whereas RISE indicates negligible relative energy error ($< 10^{-5}$) for r ≥ 5. Drastic increases for r ≤ 3 highlight the loss of late-time accuracy in very low-order models.

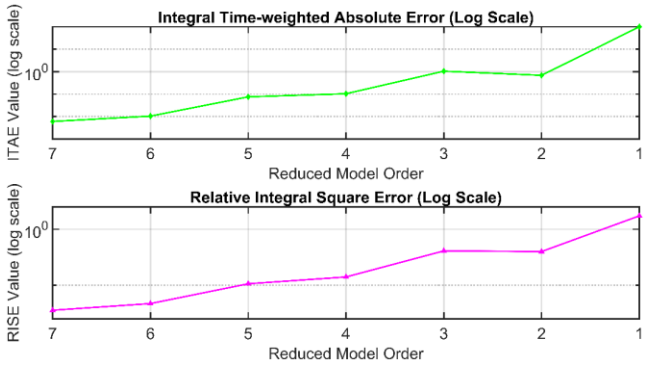

Fig. 5. ITAE and RISE vs. model order

PP-MOR yields near-perfect approximations for orders ≥ 5 in both frequency- and time-domain metrics. Orders 2 to 4 begin to show minor resonance distortion but maintain acceptable bandwidth, whereas order 1 sacrifices dynamics entirely in favor of stability and simplicity. For practical control design of this electro-mechanical system, a reduced order of 4 or 5 offers the best trade-off between model complexity and dynamic fidelity.

In the application of the PP-MOR algorithm for reducing the order of the EMRS, it is essential to balance several critical factors to identify the optimal reduced-order model. First, the reduced order should be minimized as much as possible to enhance computational efficiency, provided that the reduction does not compromise the system's fidelity. Second, the reduction error quantified by appropriate norm-based metrics should remain as low as feasible to ensure that the essential dynamics of the original high-order system are preserved. Third, the time-domain and frequency-domain responses of the reduced-order model must closely match those of the original system, thereby maintaining the accuracy of system characteristics such as transient behavior and resonance peaks. Through a systematic simulation process, we evaluated reduced models of various orders against these criteria. Based on the comprehensive assessment of reduction order, error magnitude, and response fidelity, we selected reduced models of order 1, order 2, and order 4 for further analysis and validation.

We selected reduced orders r = 1, r = 2, and r = 4 to illustrate three distinct regimes of approximation fidelity. In our error-norm analysis, orders 2 and 3 yielded nearly identical H_2, H_∞, ISE, IAE, ITAE, and RISE values, indicating that further increasing r beyond 2 yields diminishing returns. By contrast, truncation to r = 1produces a sharp jump in all error measures, especially H_∞ and ITAE, demonstrating the loss of essential resonant dynamics. The 4th-order model, however, achieves sub-10^{-3} H_∞ and H_2 errors and negligible time-domain discrepancies, effectively capturing both high- and low-frequency behavior. Thus, r = 2 represents the minimal order for acceptable accuracy, r = 1 the extreme low-order limit, and r = 4 the low-complexity point at which full-order fidelity is essentially recovered.

When reducing the original hierarchy to order 1, order 2 and order 4, we obtain the special parameters of the system on frequency and time domains as shown in Table III and Table IV.

TABLE III. FREQUENCY DOMAIN CHARACTERISTICS COMPARISON

Model order	DC Gain	Resonant Peak (Mag)	Resonant Freq. (rad/s)	Bandwidth (rad/s)
8	0	0.60599	1.00927	100
1	0.51092	0.51088	0.01000	0.87072
2	-5.55×10^{-17}	0.51089	0.99081	100
4	-8.70×10^{-17}	0.59878	0.99081	100

In Table III, we see all reduced models preserve a similar resonant peak magnitude ($\approx 0.51 \div 0.60$) and center frequency (≈ 0.99 rad/s) once order ≥ 2, indicating faithful replication of dominant resonance. Order 1 fails to capture resonance (resonant freq. shifts to 0.01 rad/s). Bandwidth and margins are also well-matched for orders ≥ 2. The infinite phase margin reflects non-oscillatory, strictly proper behavior in these SISO models. High gain margins for orders 2 and 4 (10^{15} dB) show numerical artifact of near-all-pass reduction.

TABLE IV. STEP RESPONSE CHARACTERISTICS

Model order	Rise Time (s)	Settling Time (s)	Overshoot (%)	Peak Value	Peak Time (s)	Steady State Value
8	1.668×10^{-4}	19.90	1.9141×10^{5}	0.395	1.08	2.0647×10^{-4}
1	2.5275	4.500	0	0.510	20	0.51092
2	0.02830	19.97	991.686	0.373	1.01	-1.305×10^{-8}
4	1.158×10^{-4}	19.94	2.7614×10^{5}	0.395	1.08	1.4325×10^{-4}

In the time-domain step responses presented in Fig. 6, The original system exhibits a very fast rise ($<10^{-3}$ second) but extremely large overshoot ($\approx 10^5$ %) and long settling (≈ 20 s), characteristic of under-damped second-order resonance embedded in slow modes. Reduced order 4 closely replicates these dynamics (rise $\approx 10^{-4}$ s, overshoot $\approx 2.7 \times 10^5$ %), confirming high-order fidelity. Order 2 shows excessive overshoot ($\approx 10^3$ %) but similar settling, while order 1 eliminates overshoot entirely (pure first-order behavior) yet deviates in peak time (20 second instead of ≈1 s), making it unsuitable for resonance-critical applications.

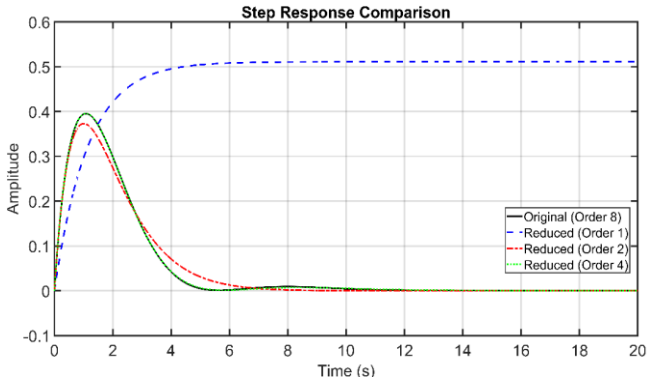

Fig. 6. Step response comparison

Step responses in Fig. 6 of the original system (solid black) and reduced models of order 1 (dashed blue), 2 (dash–dot red), and 4 (dotted green) over 20 s. The 4th-order approximation nearly overlays the full-order response, capturing both the rapid rise (≈0.0002 s) and pronounced overshoot. The 2nd-order model reproduces the resonant

peak but under-damps slightly, while the 1st-order model eliminates overshoot and slows transient timing. Consequently, the 4th-order reduced model can be recommended as a substitute for the original 8th-order system in time-domain applications.

Log–log magnitude plots in Fig. 7 for the original (solid black) and reduced systems (orders 1, 2, 4). Orders 2 and 4 show almost identical resonant peak (≈–5 dB at ≈1 rad/s) and high-frequency roll-off compared to the full model. The 1st-order approximation (blue) fails to reproduce the resonant peak and exhibits reduced bandwidth, underscoring its inadequacy for resonance-critical applications. In the frequency band from 0.5 rad/s to 2 rad/s, the amplitude response of the 2nd-order reduced model deviates noticeably from the full-order system; however, outside this band, it closely matches the original. Therefore, the 2nd-order model may replace the 8th-order system for applications outside the 0.5–2 rad/s range. Conversely, the magnitude response of the 4th-order model remains essentially indistinguishable from that of the full-order system across all frequencies.

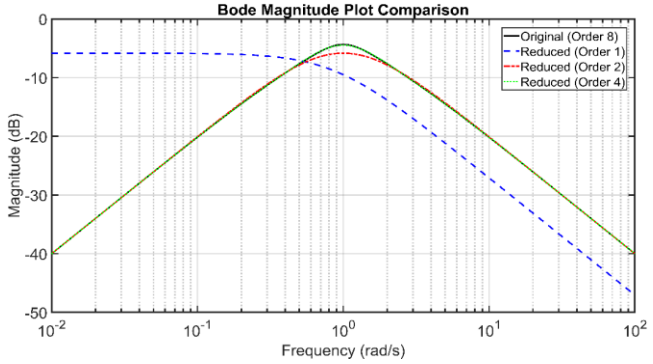

Fig. 7. Bode Magnitude plot comparison

Phase responses in Fig. 8 of the original and reduced models. Order 2 maintain phase profiles within a few degrees of the full-order system across the bandwidth, preserving phase margin. The 1st-order model displays significantly greater phase lag at mid-frequencies, indicating degraded closed-loop robustness if used for controller synthesis. Conversely, the phase response of the 4th-order model remains essentially indistinguishable from that of the full-order system across all frequencies.

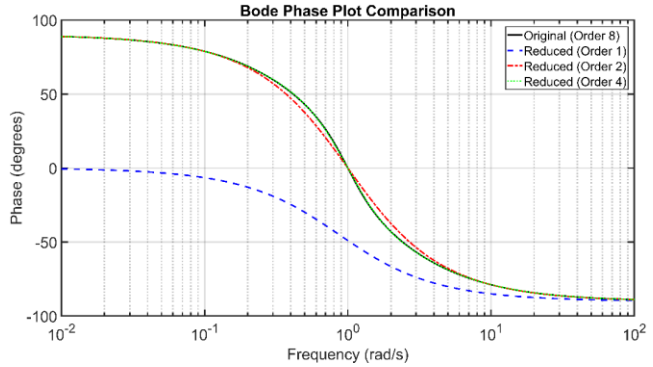

Fig. 8. Passive behavior across frequency

Over the entire frequency spectrum, both the magnitude and phase responses of the 4th-order reduced model coincide with those of the 8th-order system; hence, this reduction level is suitable for frequency-domain application.

The semilogarithmic plot in Fig. 9 illustrates the transient responses of the original eighth-order system and its reduced-order models of orders 1, 2, and 4, following an impulse disturbance introduced at $t = 5s$. The original system demonstrates a rapid decay in response magnitude, exhibiting characteristic oscillatory behavior that is increasingly well-captured as the order of the reduced model increases. The first-order reduced model significantly deviates from the original dynamics, failing to replicate both the transient peak and the subsequent decay rate. The second-order model provides a closer approximation but still underestimates the oscillatory components and the long-term decay. In contrast, the fourth-order reduced model closely follows the original trajectory across the entire time span, accurately preserving both the initial peak and the subsequent attenuation pattern. These results highlight the trade-off between model complexity and fidelity, highlighting that higher-order reduced models are essential for faithfully capturing critical transient and steady-state characteristics in the presence of impulsive disturbances.

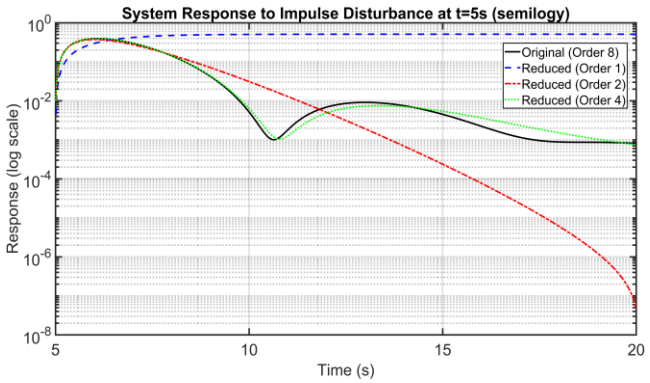

Fig. 9. System Response to Impulse Disturbance at t = 5 s

Closed-loop step response metrics reveal that the original eighth-order system achieves rapid tracking performance, with a rise time of 0.23 s, a settling time of 3.63 s, and an overshoot of approximately 11.8%. The fourth-order reduced model closely mirrors these dynamics, maintaining nearly identical rise and settling times, as well as peak and overshoot values. In contrast, the second-order model displays slightly slower settling and reduced overshoot, while the first-order model diverges substantially, exhibiting a markedly slower response and no overshoot.

The closed-loop step tracking responses depicted in Fig. 10 demonstrate that the original and fourth-order reduced models exhibit nearly indistinguishable trajectories, accurately capturing both the transient peak and the steady-state value. The second-order model approximates the original response with minor discrepancies in overshoot and settling, while the first-order model fails to replicate the system dynamics, resulting in a sluggish response and substantial steady-state error.

Fig. 11 presents the closed-loop disturbance rejection performance following a step disturbance introduced at $t = 10s$. Both the original and higher-order reduced models (orders 2 and 4) demonstrate prompt and robust disturbance

attenuation, rapidly returning to the pre-disturbance steady-state output. The first-order model, however, exhibits pronounced deviation, with slow recovery and persistent steady-state error. This comparison highlights that while moderate model reduction maintains disturbance rejection capability, excessive simplification compromises closed-loop robustness and fidelity to the original system.

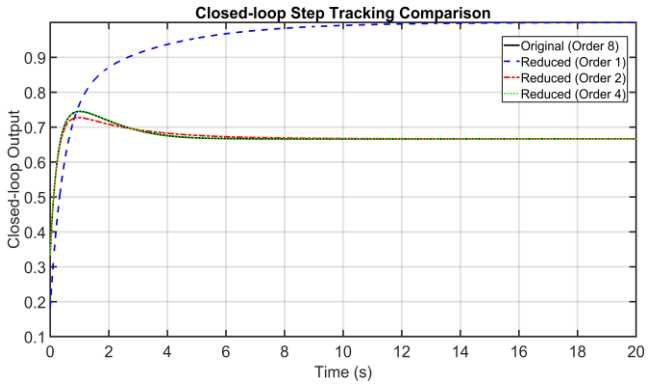

Fig. 10. Closed-loop step tracking comparison

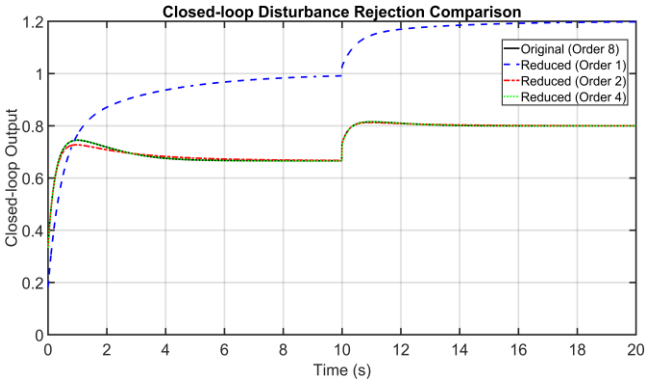

Fig. 11. Closed-loop disturbance rejection comparison

The results demonstrate that moderate-order reduced models effectively retain essential transient and steady-state characteristics, ensuring accurate closed-loop performance and disturbance rejection. In contrast, excessive reduction in model order significantly degrades system fidelity and compromises both tracking accuracy and robustness.

IV. CONCLUSION

This study advances the field of model order reduction for high-order electro-mechanical robot systems (EMRS) by developing and rigorously evaluating a passivity-preserving balanced truncation (PP-MOR) algorithm. The method systematically ensures the preservation of both stability and passivity by leveraging positive-real algebraic Riccati equations, congruence-based balancing, and explicit constraints. These theoretical contributions enable the derivation of reduced-order models that faithfully replicate the original system's frequency- and time-domain behaviors, including resonance peaks, bandwidth, phase margin, and step response overshoot.

Key findings demonstrate that the fourth-order reduced model achieves sub-10^{-3} errors in both H_2 and H_∞ norms and negligible discrepancies in time-domain indices (ISE, IAE, ITAE, RISE), closely matching the full-order system. The second-order model offers acceptable performance outside the resonance band, while the first-order model is inadequate for applications requiring dynamic fidelity. These results confirm that moderate-order reductions can dramatically lower computational complexity while retaining essential dynamic properties, facilitating efficient simulation and controller synthesis for embedded EMRS applications.

Future research will address some limitations by extending the PP-MOR framework to higher-dimensional and more complex EMRS, including flexible and nonlinear systems. It is also important to investigate the robustness of reduced-order models under parameter variations and unmodeled dynamics, potentially incorporating robust or adaptive MOR strategies. Additionally, benchmarking PP-MOR against other model order reduction methods in terms of accuracy, computational speed, and scalability, both in simulation and on embedded hardware, will provide a clearer picture of its practical advantages. Finally, future work should explore automated model order selection criteria tailored to specific application performance requirements, ensuring optimal balance between model simplicity and dynamic fidelity.

In summary, this work provides a systematic and reproducible methodology for passivity-preserving model order reduction in EMRS, bridging the gap between high-fidelity modeling and computational tractability. By clarifying the trade-offs between model complexity and dynamic fidelity, and by highlighting both the strengths and limitations of the PP-MOR approach, the article contributes valuable insights and practical tools to the design and deployment of advanced robotic systems. The findings and proposed future directions lay a solid foundation for further innovation in scalable, robust, and energy-aware control of electro-mechanical robots.

FUNDING

This research received no external funding.

ACKNOWLEDGMENT

The authors gratefully acknowledge Thai Nguyen University of Technology, Vietnam, for supporting this work.

REFERENCES

[1] S. A. Al-Samarraie and I. I. Gorial, "Modeling of electromechanical system and motion control for mechatronics application," *Int Rev Automat Control*, vol. 16, pp. 246-252, 2023.

[2] E. Clochiatti, L. Scalera, P. Boscariol, and A. Gasparetto, "Electro-mechanical modeling and identification of the UR5 e-series robot," *Robotica*, vol. 42, no. 7, pp. 2430-2452, 2024.

[3] C. M. Pappalardo and D. Guida, "Modeling an industrial robotic manipulator in the electromechanical domain," *Contemporary Materials*, vol. 14, no. 2, 2023.

[4] A. Alrumayh, K. Alhassoon, F. Alsaleem, M. Shaban, and F. N. Alsunaydih, "Electromagnetically Driven Robot for Multipurpose Applications," *Applied Sciences*, vol. 15, no. 2, p. 973, 2025.

[5] W. Zhang, "Electromechanical Coupling Characteristics Analysis and Research of Rotation-Parallel Flexible Robot Manipulator," *researchsquare*, 2022.

[6] Q. Fang, Y. Zhou, S. Ma, C. Zhang, Y. Wang, and H. Huangfu, "Electromechanical actuator servo control technology based on active disturbance rejection control," *Electronics*, vol. 12, no. 8, p. 1934, 2023.

[7] G. E. Fúnez, A. M. Carrasco, and J. L. Ordoñez-Ávila, "Study Case: Electromechanical Design of a Magnetic Damper for Robotic Systems," *Int. J. Mech. Eng. Robot. Res*, vol. 10, pp. 66-72, 2022.

[8] Z. Traina. *U.S. Patent No. 11,730,552*. Washington, DC: U.S. Patent and Trademark Office, 2023.

[9] J. Zeng and Y. Zeng, "Application of robot in handling electric field short-circuit fault of electrostatic precipitator without stopping," in *5th International Conference on Information Science, Electrical, and Automation Engineering (ISEAE 2023)*, vol. 12748, pp. 698-706, 2023.

[10] S. Hogipuram, V. K. Gunti, and R. Kumar, "Design of SoC based Compact, High Bandwidth Electro-Mechanical Actuation (EMA) System for Aerospace Application," in *2022 International Conference for Advancement in Technology (ICONAT)*, pp. 1-7, 2022.

[11] Ö. N. Cora and M. E. Şahin, "Turkish Journal of Electromechanics & Energy in Its Fifth Year, and Portrait of a Pioneer in Engineering: Al-Jazari," *Turkish Journal of Electromechanics and Energy*, vol. 5, no. 1, 2020.

[12] B. Guan, R. V. Godoy, F. Sanches, A. Dwivedi, and M. Liarokapis, "On semi-autonomous robotic telemanipulation employing electromyography based motion decoding and potential fields," in *2023 IEEE/RSJ International Conference on Intelligent Robots and Systems (IROS)*, pp. 6991-6997, 2023.

[13] Y. Zhang *et al*., "Coaxially printed magnetic mechanical electrical hybrid structures with actuation and sensing functionalities," *Nature communications*, vol. 14, no. 1, p. 4428, 2023.

[14] P. Lancaster, C. Mavrogiannis, S. Srinivasa, and J. R. Smith, "Electrostatic brakes enable individual joint control of underactuated, highly articulated robots," *The International Journal of Robotics Research*, vol. 43, no. 14, pp. 2204-2220, 2024.

[15] I. D. Sîrbu *et al*., "Electrostatic bellow muscle actuators and energy harvesters that stack up," *Science Robotics*, vol. 6, no. 51, p. eaaz5796, 2021.

[16] T. E. Amish, J. T. Auletta, C. C. Kessens, J. R. Smith, and J. I. Lipton, "Electrostatic Clutches Enable Simultaneous Mechanical Multiplexing," *arXiv preprint arXiv:2501.08469*, 2025, doi: 10.48550/arxiv.2501.08469.

[17] P. Lancaster, P. Gyawali, C. Mavrogiannis, S. S. Srinivasa and J. R. Smith, "Optical Proximity Sensing for Pose Estimation During In-Hand Manipulation," *2022 IEEE/RSJ International Conference on Intelligent Robots and Systems (IROS)*, pp. 11818-11825, 2022.

[18] H. Jing, Q. Lin, M. Liu, and H. Liu, "Electromechanical braking systems and control technology: A survey and practice," *Proceedings of the Institution of Mechanical Engineers, Part D: Journal of Automobile Engineering*, p. 09544070241271826, 2024.

[19] J. Hwang *et al*., "An Electromagnetically Controllable Microrobotic Interventional System for Targeted, Real-Time Cardiovascular Intervention (Adv. Healthcare Mater. 11/2022)," *Advanced Healthcare Materials*, vol. 11, no. 11, p. 2270062, 2022.

[20] B. I. Oladapo *et al*., "Experimental analytical design of CNC machine tool SCFC based on electro-pneumatic system simulation," *Engineering Science and Technology, an International Journal*, vol. 19, no. 4, pp. 1958-1965, 2016.

[21] T. Bhatta, G. B. Pradhan, S. Lee, and J. Y. Park, "An electromagnetic and triboelectric hybrid motion sensing system for self-powered robotic balancing platforms," in *2022 21st International Conference on Micro and Nanotechnology for Power Generation and Energy Conversion Applications (PowerMEMS)*, pp. 75-78, 2022.

[22] H. Wang, Y. Jiang, C. Qi, and J. Li, "Research on Integrated Electro-mechanical (EMA) Servo System," in *2020 IEEE Conference on Telecommunications, Optics and Computer Science (TOCS)*, pp. 195-198, 2020.

[23] J. Li and Y. Jiang, "Variable Universe Fuzzy–Proportional-Integral-Differential-Based Braking Force Control of Electro-Mechanical Brakes for Mine Underground Electric Trackless Rubber-Tired Vehicles," *Sensors*, vol. 24, no. 9, p. 2739, 2024.

[24] H. G. Song and D. W. Lim, "Application of the Water-Based Electro-Hydraulic Actuator (EHA) to the Heavy-Duty Collaborative Robot," in *Actuators*, vol. 13, no. 11, p. 451, 2024.

[25] G. Menaka, V. Horpyati, A. S. K. Reddy, M. Awasthy, and S. KS, "Automated Electric Arm with FPGA Processor and Embedded Systems," in *2023 IEEE International Conference on Integrated Circuits and Communication Systems (ICICACS)*, pp. 1-7, 2023.

[26] Y. S. Paranchuk and Y. V. Shabatura, "Electromechanical guidance system based on a fuzzy proportional-plus-differential position controller," *Электротехника и электромеханика*, no. 3, pp. 25-31, 2021.

[27] T. Boz, İ. Aras, S. Kıkıcı, and S. Ersoy, "Electronic and mechanical design of a hexapod land searching robot," *International Advanced Researches and Engineering Journal*, vol. 4, no. 1, pp. 34-40, 2020.

[28] H. Askari, Z. Saadatnia, E. Asadi, A. Khajepour, M. B. Khamesee, and J. Zu, "A flexible hybridized electromagnetic-triboelectric multi-purpose self-powered sensor," *Nano Energy*, vol. 45, pp. 319-329, 2018.

[29] R. Crowder, *Electric drives and electromechanical systems: applications and control*, Butterworth-Heinemann, 2019.

[30] Z. Liu, J. Sun, D. Yue, X. Zuo, H. Gao, and K. Feng, "A review on integral evolution of electro-hydraulic actuation in three momentous domains: aerospace, engineering machinery, and robotics," in *Fourth International Conference on Mechanical Engineering, Intelligent Manufacturing, and Automation Technology (MEMAT 2023)*, vol. 13082, pp. 141-159, 2024.

[31] Z. Tian *et al*., "A mechanical manipulated electromechanical coupling design with stretchable electret film: mechanical sensing, energy harvesting, and actuation," *Smart Materials and Structures*, vol. 33, no. 6, p. 065031, 2024.

[32] S. A. Shaqaq, "Advanced Electromagnetic Wheel Robot," in *2022 7th International Conference on Mechanical Engineering and Robotics Research (ICMERR)*, pp. 69-72, 2022.

[33] A. Chaudhuri, R. Datta, M. P. Kumar, J. P. Davim, and S. Pramanik, "Energy conversion strategies for wind energy system: Electrical, mechanical and material aspects," *Materials*, vol. 15, no. 3, p. 1232, 2022.

[34] H. Shigemune, K. Pradidarcheep, Y. Kuwajima, Y. Seki, S. Maeda, and V. Cacucciolo, "Wireless electrohydrodynamic actuators for propulsion and positioning of miniaturized floating robots," *Advanced Intelligent Systems*, vol. 3, no. 7, p. 2100004, 2021.

[35] O. Nazarova *et al*., "Mechatronic automatic control system of electropneumatic manipulator," *Scientific Reports*, vol. 14, no. 1, p. 6970, 2024.

[36] C. Liu, O. Edwards, K. Althoefer, K. Zhang, and H. Godaba, "An electro-pneumatic shape morphing rolling robot with variable locomotion modes," in *2022 IEEE 5th International Conference on Soft Robotics (RoboSoft)*, pp. 715-721, 2022.

[37] N. Jayasekara *et al*., "Revolutionizing Accessibility: Smart Wheelchair Robot and Mobile Application for Mobility, Assistance, and Home Management," *Journal of Robotics and Control (JRC)*, vol. 5, no. 1, pp. 27-53, 2024.

[38] E. A. Nugroho, J. D. Setiawan, and M. Munadi, "Handling four DOF robot to move objects based on color and weight using fuzzy logic control," *Journal of Robotics and Control (JRC)*, vol. 4, no. 6, pp. 769-779, 2023.

[39] L. Yang, N. Guo, R. Sakamoto, N. Kato, and K. I. Yano, "Electric wheelchair hybrid operating system coordinated with working range of a robotic arm," *Journal of Robotics and Control (JRC)*, vol. 3, no. 5, pp. 679-689, 2022.

[40] Z. Anjum, S. Samo, A. Nighat, A. U. Nisa, M. A. Soomro, and R. Alayi, "Design and Modeling of 9 Degrees of Freedom Redundant Robotic Manipulator," *Journal of Robotics and Control (JRC)*, vol. 3, no. 6, pp. 800-808, 2022.

[41] P. Chotikunnan, R. Chotikunnan, and P. Minyong, "Adaptive parallel iterative learning control with a time-varying sign gain approach empowered by expert system," *Journal of Robotics and Control (JRC)*, vol. 5, no. 1, pp. 72-81, 2024.

[42] K. Yamtuan, T. Radomngam, and P. Prempraneerach, "Visual servo kinematic control of delta robot using YOLOv5 algorithm," *Journal of Robotics and Control (JRC)*, vol. 4, no. 6, pp. 818-831, 2023.

[43] H. Yadavari, V. T. Aghaei, and S. I. GLU, "Addressing challenges in dynamic modeling of stewart platform using reinforcement learning-based control approach," *Journal of Robotics and Control (JRC)*, vol. 5, no. 1, pp. 117-131, 2024.

[44] R. D. Puriyanto and A. K. Mustofa, "Design and implementation of fuzzy logic for obstacle avoidance in differential drive mobile robot," *Journal of Robotics and Control (JRC)*, vol. 5, no. 1, pp. 132-141, 2024.

[45] T. Q. Ngo, T. H. Tran, T. T. H. Le, and B. M. Lam, "An application of modified T2FHC algorithm in two-link robot controller," *Journal of Robotics and Control (JRC)*, vol. 4, no. 4, pp. 509-520, 2023.

[46] J. Díaz-Téllez, R. S. García-Ramírez, J. Pérez-Pérez, J. Estevez-Carreón, and M. A. Carreón-Rosales, "ROS-based Controller for a Two-Wheeled Self-Balancing Robot," *Journal of Robotics and Control (JRC)*, vol. 4, no. 4, pp. 491-499, 2023.

[47] O. Y. Ismael, M. Almaged, and A. I. Abdulla, "Nonlinear model predictive control-based collision avoidance for mobile robot," *Journal of Robotics and Control (JRC)*, vol. 5, no. 1, pp. 142-151, 2024.

[48] R. Pyla, V. Pandalaneni, and P. J. N. Raju, "Design and development of swarm AGV's alliance for search and rescue operations," *Journal of Robotics and Control (JRC)*, vol. 4, no. 6, pp. 791-807, 2023.

[49] N. M. Alyazidi, A. M. Hassanine, M. S. Mahmoud, and A. Ma'arif, "Enhanced Trajectory Tracking of 3D Overhead Crane Using Adaptive Sliding-Mode Control and Particle Swarm Optimization," *Journal of Robotics and Control (JRC)*, vol. 5, no. 1, pp. 253-262, 2024.

[50] T. Q. Ngo, T. T. H. Le, B. M. Lam, and T. K. Pham, "Adaptive Single-Input Recurrent WCMAC-Based Supervisory Control for De-icing Robot Manipulator," *Journal of Robotics and Control (JRC)*, vol. 4, no. 4, pp. 438-451, 2023.

[51] D. T. Tran, N. M. Hoang, N. H. Loc, Q. T. Truong, and N. T. Nha, "A fuzzy LQR PID control for a two-legged wheel robot with uncertainties and variant height," *Journal of Robotics and Control (JRC)*, vol. 4, no. 5, pp. 612-620, 2023.

[52] M. H. Widianto and B. Juarto, "Smart Farming Using Robots in IoT to Increase Agriculture Yields: A Systematic Literature Review," *Journal of Robotics and Control (JRC)*, vol. 4, no. 3, pp. 330-341, 2023.

[53] R. K. Salih and W. S. Aboud, "Smart Robotic Exoskeleton: Constructing Using 3D Printer Technique for Ankle-Foot Rehabilitation," *Journal of Robotics and Control (JRC)*, vol. 4, no. 4, pp. 537-547, 2023.

[54] P. Chotikunnan and Y. Pititheeraphab, "Adaptive p control and adaptive fuzzy logic controller with expert system implementation for robotic manipulator application," *Journal of Robotics and Control (JRC)*, vol. 4, no. 2, pp. 217-226, 2023.

[55] W. Al-Mayahi and H. Al-Fahaam, "A novel variable stiffness compound extensor-pneumatic artificial muscle (ce-pam): Design and mathematical model," *Journal of Robotics and Control (JRC)*, vol. 4, no. 3, pp. 342-355, 2023.

[56] M. Auzan, D. Lelono, and A. Dharmawan, "Humanoid walking control using lqr and anfis," *Journal of Robotics and Control (JRC)*, vol. 4, no. 4, pp. 548-556, 2023.

[57] V. V. Kravchenko *et al*., "Mathematical model of a robot-spider for group control synthesis: Derivation and validation," *Journal of Robotics and Control (JRC)*, vol. 4, no. 6, pp. 849-855, 2023.

[58] M. Fazilat and N. Zioui, "The impact of simplifications of the dynamic model on the motion of a six-jointed industrial articulated robotic arm movement," *Journal of Robotics and Control (JRC)*, vol. 5, no. 1, pp. 173-186, 2024.

[59] V. V. Kravchenko *et al*., "Comparison of Spider-Robot Information Models," *Journal of Robotics and Control (JRC)*, vol. 4, no. 5, pp. 719-725, 2023.

[60] V. D. Cong, "Path following and avoiding obstacle for mobile robot under dynamic environments using reinforcement learning," *Journal of Robotics and Control (JRC)*, vol. 4, no. 2, pp. 157-164, 2023.

[61] N. X. Chiem, "Synthesis of LQR Controller Based on BAT Algorithm for Furuta Pendulum Stabilization," *Journal of Robotics and Control (JRC)*, vol. 4, no. 5, pp. 662-669, 2023.

[62] A. Irawan, M. I. P. Azahar, and D. Pebrianti, "Interaction Motion Control on Tri-finger Pneumatic Grasper using Variable Convergence Rate Prescribed Performance Impedance Control with Pressure-based Force Estimator," *Journal of Robotics and Control (JRC)*, vol. 3, no. 5, pp. 716-724, 2022.

[63] A. Voelz, D. Kiesenhofer, and D. Karagiannis, "Decreasing the Design Complexity of Cyber-Physical Systems through Conceptual Modeling: The Robot Abstraction Method," in *2024 IEEE 10th World Forum on Internet of Things (WF-IoT)*, pp. 1-7, 2024.

[64] D. Karamzin, "On the study of higher-order state-constrained control systems," in *2024 10th International Conference on Control, Decision and Information Technologies (CoDIT)*, pp. 2061-2065, 2024.

[65] Y. Wei, X. Liu, J. Kong, Z. Cheng, and W. Fang, "A New MRACS Approach for High-order System Following Low-order Model Using State Variables Taking from the Model," in *2024 International Conference on Advanced Control Systems and Automation Technologies (ACSAT)*, pp. 238-241, 2024.

[66] M. Li, W. Bian, L. Chen, and M. Liu, "HiDeS: a higher-order-derivative-supervised neural ordinary differential equation for multi-robot systems and opinion dynamics," *Frontiers in Neurorobotics*, vol. 18, p. 1382305, 2024.

[67] W. Xia, Y. Wang, Y. Hao, Z. He, K. Yan, and F. Zhao, "Reliability analysis for complex electromechanical multi-state systems utilizing universal generating function techniques," *Reliability Engineering & System Safety*, vol. 244, p. 109911, 2024.

[68] Y. Wang, A. Li, and L. Wang, "Networked dynamic systems with higher-order interactions: stability versus complexity," *National Science Review*, vol. 11, no. 9, 2024.

[69] Y. Li, X. Yao, and B. Ma, "Event-triggered optimal interaction control of the MRM system under the complex multi-task constraints: design and experiments," *Journal of the Franklin Institute*, vol. 360, no. 2, pp. 910-942, 2023.

[70] T. G. Molnar and A. D. Ames, "Safety-critical control with bounded inputs via reduced order models," in *2023 American Control Conference (ACC)*, pp. 1414-1421, 2023.

[71] A. Podlubne, J. Mey, S. Pertuz, U. Aßmann, and D. Göhringer, "Model-based generation of hardware/software architectures for robotics systems," in *2022 32nd International Conference on Field-Programmable Logic and Applications (FPL)*, pp. 153-159, 2022.

[72] D. Karamzin and F. L. Pereira, "On higher-order state constraints," *SIAM Journal on Control and Optimization*, vol. 61, no. 4, pp. 1913-1933, 2023.

[73] A. Jansma, "A Compositional Approach to Higher-Order Structure in Complex Systems: Carving Nature at its Joints," *arXiv e-prints, arXiv-2404*, 2024.

[74] F. Bonilla, T. Holzer, and S. Sarkani, "Complexity measure for engineering systems incorporating system states and behavior," *IEEE Systems Journal*, vol. 15, no. 4, pp. 4792-4803, 2020.

[75] L. H. Ma, Y. B. Zhong, G. D. Wang, and N. Li, "The Kinematic and Dynamic Modeling and Numerical Calculation of Robots with Complex Mechanisms Based on Lie Group Theory," *Mathematical Problems in Engineering*, vol. 2021, no. 1, p. 6014256, 2021.

[76] P. S. Oruganti, P. Naghizadeh, and Q. Ahmed, "Safe control using high-order measurement robust control barrier functions," in *2023 American Control Conference (ACC)*, pp. 4148-4154, 2023.

[77] Y. Chen, X. Li, Y. Liang, Z. Shi, and Z. Song, "The computational limits of state-space models and mamba via the lens of circuit complexity," *arXiv preprint arXiv:2412.06148*, 2024.

[78] Z. Salehi, P. Karimaghaee, and M. H. Khooban, "A new passivity preserving model order reduction method: conic positive real balanced truncation method," *IEEE Transactions on Systems, Man, and Cybernetics: Systems*, vol. 52, no. 5, pp. 2945-2953, 2021.

[79] I. Dorschky, T. Reis, and M. Voigt, "Balanced truncation model reduction for symmetric second order systems---a passivity-based approach," *SIAM Journal on Matrix Analysis and Applications*, vol. 42, no. 4, pp. 1602-1635, 2021.

[80] N. Wong and V. Balakrishnan, "Fast positive-real balanced truncation via quadratic alternating direction implicit iteration," *IEEE Transactions on Computer-Aided Design of Integrated Circuits and Systems*, vol. 26, no. 9, pp. 1725-1731, 2007.

[81] K. Unneland, P. Van Dooren, and O. Egeland, "A novel scheme for positive real balanced truncation," in *2007 American Control Conference*, pp. 947-952, 2007.

[82] A. K. Prajapati and R. Prasad, "Model reduction using the balanced truncation method and the Padé approximation method," *IETE Technical Review*, vol. 39, no. 2, pp. 257-269, 2022.

[83] C. Yang, Z. Fan and Y. Xia, "Convex Model-Based Reduced-Order Model for Uncertain Control Systems," in *IEEE Transactions on Systems, Man, and Cybernetics: Systems*, vol. 54, no. 7, pp. 4236-4246, July 2024.

[84] Z. Salehi, P. Karimaghaee, S. Salehi, and M. H. Khooban, "Phase Preserving Balanced Truncation for Order Reduction of Positive Real Systems," *Automation*, vol. 3, no. 1, pp. 84-94, 2022.

[85] Z. Salehi, P. Karimaghaee, and M. H. Khooban, "Model order reduction of positive real systems based on mixed gramian balanced truncation with error bounds," *Circuits, Systems, and Signal Processing*, vol. 40, no. 11, pp. 5309-5327, 2021.

[86] Z. Salehi, P. Karimaghaee, and M. H. Khooban, "Mixed positive-bounded balanced truncation," *IEEE Transactions on Circuits and Systems II: Express Briefs*, vol. 68, no. 7, pp. 2488-2492, 2021.

[87] S. Choudhary, V. H. Gaidhane and V. Naranje, "Analysis of Flexible Aircraft Design Using Reduced Order Modelling," *2023 International Conference on Computational Intelligence and Knowledge Economy (ICCIKE)*, pp. 355-360, 2023.

[88] D. Kumar *et al*., "Positive-real truncated balanced realization based frequency-weighted model reduction," in *2019 Australian & New Zealand Control Conference (ANZCC)*, pp. 145-147, 2019.

[89] Y. Tanji, "Reciprocal and Positive Real Balanced Truncations for Model Order Reduction of Descriptor Systems," *arXiv preprint arXiv:1811.04630*, 2018.

[90] S. Mahata, N. Herencsar, B. B. Alagoz and C. Yeroglu, "A Robust Frequency-Domain-Based Order Reduction Scheme for Linear Time-Invariant Systems," in *IEEE Access*, vol. 9, pp. 165773-165785, 2021.

[91] T. K. Maiti, D. Navarro, M. Miura-Mattausch and H. J. Mattausch, "Compact modeling approach for electro-mechanical system simulation," in *2017 IEEE 12th International Conference on ASIC (ASICON)*, pp. 981-984, 2017.

[92] S. Dutta *et al*., "Self-controlled walking robot with gyro sensor network for stable movement on non-smooth surfaces," in *2018 IEEE International Conference on Simulation, Modeling, and Programming for Autonomous Robots (SIMPAR)*, pp. 137-143, 2018.